Magnetocapacitance of a three-probe mesoscopic capacitor

Haiqing Wei and Ningjia Zhu
Center for the Physics of Materials and Department of Physics, McGill University, Montreal, Quebec, Canada H3A 2T8

Jian Wang
Department of Physics, The University of Hong Kong, Pokfulam Road, Hong Kong, China

Hong Guo
Center for the Physics of Materials and Department of Physics, McGill University, Montreal, Quebec, Canada H3A 2T8
(Received 23 October 1996)

We report a numerical calculation of the magnetocapacitance for a three-probe capacitor and investigate the asymmetry property of the electrochemical capacitance under a magnetic-field reversal. At low magnetic fields the quantum magnetocapacitance shows a large asymmetry under a field reversal. At higher fields the capacitance is dominated by Aharonov-Bohm type oscillations and the fluctuations of the asymmetry is reduced. [S0163-1829(97)00139-2]

The physics associated with quantum conduction in various very small and low-dimensional systems has been a main focus in recent years. Due to spatial quantization, the physical behavior of these nanostructures is very different from their classical counterpart. In particular, it has been understood that in mesoscopic length scales, the classical notion of electrostatic capacitance, $C_e \equiv dQ/dU$, may not be useful.[1] Instead one introduces the concept of electrochemical capacitance, $C_\mu \equiv e dQ/d\mu$, which is a quantity depending on the properties of the conductor.[1] The reason these two capacitances can differ significantly at mesoscopic length scale is because the electrostatic potential drop (dU) at the capacitor plates can be very different from the voltage drop ($d\mu/e$) in the electron reservoirs. The electrochemical capacitance has played a relevant role in several experiments, especially those using capacitance spectroscopy.[2] In a recent experiment, Chen *et al.*[3] have measured the magnetic-field symmetry properties of the capacitance tensor for several multiprobe two-dimensional (2D) systems, and found large and almost complete asymmetry under field reversal. This property has been anticipated from the point of view of a current conserving and gauge invariant ac-transport theory proposed by Büttiker and co-workers.[1,4] Despite this systematic formulation,[1] which provided the general understanding of the symmetry properties of electrochemical capacitance,[4] to the best of our knowledge we are not aware of practical calculations of the mesoscopic capacitance in 3D using this formalism. It is clear that practical calculations of various mesoscopic capacitance and investigating their behavior are very important problems that warrant detailed effort. The purpose of this paper is to report our work in this direction.

In particular, we have numerically calculated the mesoscopic capacitance of a three-probe device, shown in Fig. 1, using the current conserving formalism of Ref. 1. The system consists of a two-probe mesoscopic semiconductor plate with a size 3300 Å$\times$3300 Å. It connects to reservoirs 1 and 2 through two quantum wires with the same width $w = 1650$ Å. The potential $U(\mathbf{r})$ inside the plate is zero except at the boundary of the plate, where it is assumed to be infinite. The second plate of the capacitor is assumed to be a large metal gate on top of the mesoscopic plate, and the third probe resides on the metal gate. Between the plates there is an insulating layer with a thickness 1000 Å. The whole system, including the leads, is inside a uniform magnetic field and we shall focus on investigating the magnetic-field dependence of the capacitance. The system studied here has more than a mere academic interest. Indeed, in quantum devices fabricated via the split gate technology, the devices are near various metal gates. Hence it is necessary to understand the capacitive coupling of the devices to the metal gates. Since the system has two terminals (1 and 2) that are not coupled purely capacitively, we expect that the capacitance C_{31} to be asymmetric with respect to a magnetic-field reversal.[3,4] Indeed, we found that the capacitance shows an asymmetry under field reversal for the whole range of field strengths we have studied. At the higher fields range the magnetocapacitance is dominated by Aharonov-Bohm type oscillations, which are less sensitive to the field reversal and the asymmetric fluctuations of the capacitance are reduced.

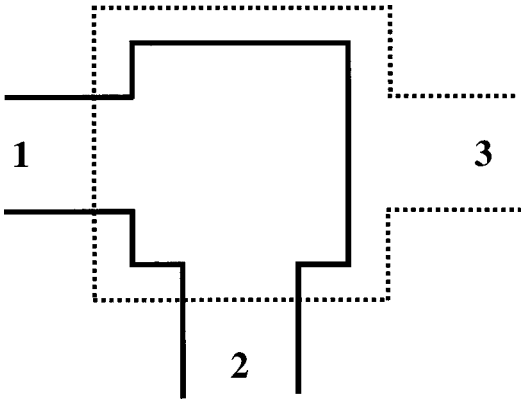

FIG. 1. Sketch of the three-probe system. Probes 1 and 2 are connected to the middle of the 3300$\times$3300 Å semiconductor plate (solid lines), with width $w = 1650$ Å. The dotted line is a very large classical metal plate on top of the seconductor plate. The distance between the two parallel plates is kept at 1000 Å.

Generally, a change of electrochemical potential in one reservoir leads to very complicated effects.[5] The semiconductor plate may be charged, or may remain neutral but polarized due to compensating responses of other reservoirs. However, for very small sizes of the semiconductor plate the plate will be charged. In this case it is reasonable to assume that an increment of the electrochemical potential $d\mu_j$ ($j=1,2$) at reservoir j injects an additional carrier density $d\rho_j(\mathbf{r})$ into the semiconductor plate,

$$d\rho_j(\mathbf{r})=\left[\frac{dn(\mathbf{r},j)}{dE}\right]d\mu_j, \tag{1}$$

where $dn(\mathbf{r},j)/dE$ is the *injectivity* of contact j. By the free-electron scattering approach[6] the injectivity is related to the scattering wave function,

$$\frac{dn(\mathbf{r},j)}{dE}=\sum_n \frac{|\Psi_{jn}(\mathbf{r})|^2}{h v_{jn}}. \tag{2}$$

Here v_{jn} is the velocity of incident carriers in channel n in contact j. With the injected charge as determined by the injectivity, in principle one can solve,[1] for our problem, a three-dimensional self-consistent equation for the *characteristic potential* $u_j(\mathbf{r})$, which describes the variation of the potential landscape due to a change of the electrochemical potential at contact j. The self-consistency comes in because one has to determine the induced charge inside the system. The characteristic potential is determined by the Poisson equation,[1]

$$\nabla^2 u_j(\mathbf{r})=-4\pi[\rho_j(\mathbf{r})+\rho_{\rm ind}(\mathbf{r})], \tag{3}$$

where ρ_j is the injected charge through contact j. $\rho_{\rm ind}$ is the induced charge, which is related to a complicated Lindhard function convoluted with the characteristic potential.[7] Thus a self-consistent solution of this equation solves the induced charge.[1] We shall be interested in the behavior of capacitance C_{3j} as a function of the magnetic field B. Hence it is necessary to determine the induced charge at the metal gate when external charges are injected from contacts $j=1,2$. Because the electron density of states is very large in the metal gate, the response of the gate can be approximately treated classically. Thus instead of solving Eq. (3) self-consistently to determine $\rho_{\rm ind}$, we simply assume that there is an image charge density in the metal gate. The capacitance C_{31} and C_{32} are defined as $C_{3j}=edQ_3/d\mu_j$, $j=1,2$, where dQ_3 is the electric charge (the induced charge) accumulation on the metal gate due to the increase of the chemical potential $d\mu_j$ at contacts $j=1,2$. Treating the gate *classically* means it merely provides an image charge to the injected charge on the semiconductor plate. We thus obtain $dQ_3=-dQ_1$ for a change of electrochemical potential at the first contact, $d\mu_1$. This allows us to obtain the electrochemical capacitance C_{31}. We caution that this procedure is reasonable only when the second plate is a large metal. If not, then a direct calculation of the charge dQ_3 will be needed by solving Eq. (3). Since our primary concern is the magnetic-field asymmetry property of the eletrochemical capacitance, our model is adequate.

With the classical treatment of the metal gate, quantum mechanics enters in the calculation of the injectivity of Eq. (2). This can be done in two ways. In the first method, we solve the free-electron scattering problem for electrons coming from contacts $j=1,2$ with the model confinement potential $U(\mathbf{r})$ described above. The solution gives the scattering wave function $\psi_{jn}(\mathbf{r})$ by which we obtain the injectivity from Eq. (2). Then through Eq. (1) we obtain the injected charge density $d\rho_j(\mathbf{r})$, which in turn determines $dQ_j=\int d\mathbf{r}[d\rho_j(\mathbf{r})]$. In the second method, which is a slightly more refined procedure, we can include the changes of the scattering potential $U(\mathbf{r})$ due to the scattering electron wave functions. For this purpose we notice that the injected charge $d\rho_j(\mathbf{r})$ and its image charge on the metal gate give rise to an extra potential $dU(\mathbf{r})$, which modifies the scattering potential from the original $U(\mathbf{r})$ to $U(\mathbf{r})+dU(\mathbf{r})$. This in turn affects the injectivity: thus we have a self-consistent problem that we can solve numerically to account for the effects of dU. At the end of this self-consistency, when the system reaches the new equilibrium that corresponds to the proper characteristic potential, there is a charge density $dn_j(\mathbf{r})$ inside the semiconductor plate. Again, integrating dn_j we obtain the charge dQ_j due to the raise of $d\mu_j$. We comment that $dU(\mathbf{r})$ should only be a small correction to $U(\mathbf{r})$ because for small $d\mu_j$, the injected charge that causes dU is small. This slightly refined calculation gives a small correction to the injectivity. However near a quantum resonance mediated by a quasibound state, as shown in Ref. 8 the effect of dU can be substantial. Finally, after determining dQ_j,[9] for our model we thus obtain $dQ_3=-dQ_j$, and find $C_{3j}=edQ_3/d\mu_j$. In order to obtain the injectivity, we solve the Schrödinger equation for the scattering problem by a finite-element numerical scheme discussed in detail in Ref. 10 that gives the wave function inside the scattering region as well as the transmission coefficients.[12]

While only a technical point, we briefly outline the determination of dU and of $dn_j(\mathbf{r})$. We start from the injected charge density from probe j, $d\rho_j(\mathbf{r})$ of Eq. (1). Because the metal gate is assumed to respond classically, it instantly provides an image charge of the same amount (differ by a sign). As a second step we calculate the induced electric potential $dU(\mathbf{r})$ from classical electrodynamics, i.e., Coulomb's law,

$$dU(\mathbf{r})=\int \frac{ed\rho(\mathbf{r}')}{\epsilon|\mathbf{r}-\mathbf{r}'|}. \tag{4}$$

Here $d\rho(\mathbf{r})$ represents both the injected charge in the semiconductor and its image charge on the metal gate, and ϵ is the dielectric constant. In principle, we should solve a Poisson equation to obtain dU by imposing appropriate electrostatic boundary conditions at the three reservoirs. However, to apply the current conserving theoretical formalism[1] we must set the chemical potential change $d\mu_j$ very small, hence a direct integration of Eq. (4) is adequate for our purpose. In the third step we put this potential variation $dU(\mathbf{r})$ into the scattering region, and solve the scattering problem again with the new potential $U(\mathbf{r})+dU(\mathbf{r})$. This leads to a more refined charge density $d\rho_j$. Such a procedure is repeated until convergence. In our calculations we usually obtained convergence in only a few iterations.

It is well known[11] that for systems such as our two-probe semiconductor plate, the resistance is symmetric under magnetic-field reversal, i.e., $R(\mathbf{B})=R(-\mathbf{B})$. The electro-

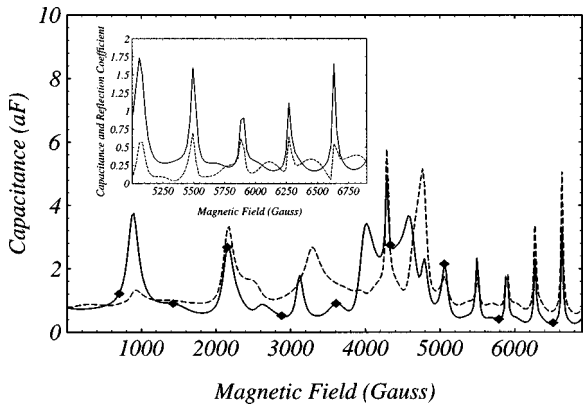

FIG. 2. The capacitance (in FF) of the two parallel plates of Fig. 1 as a function of an external magnetic field **B**. Solid line, $C_{31}(\mathbf{B})$; dashed line, $C_{31}(-\mathbf{B})$. Both these quantities were computed only using the injected charge. Data points, $C_{31}(\mathbf{B})$ computed using the self-consistently determined charge density $dn_j(\mathbf{r})$. The two calculations differ by about 1% in the values. Inset: comparison of the first subband contribution to $C_{31}(\mathbf{B})$ (solid line) with the reflection coefficient (dashed line). The peak positions are well aligned.

chemical capacitance between the plate and the metal gate (a three-probe system), however, is generally asymmetric under the field reversal.[4] This is easy to understand since the scattering wave functions are usually sensitive to the direction of the magnetic field, thus from Eq. (2) so is the injectivity that essentially determines the capacitance. We have fixed the incoming electron energy $E \equiv \hbar^2/(2m^*)k^2$ by specifying $kw = 9.5$, which is just above the third propagation subband without B. Here k is the momentum of the incoming electron, $\hbar$ the Planck constant divided by 2π, m^* is the effective mass of the electron and w is the width of the probe. With $w = 1650$ Å, the energy threshold of the first subband is 0.207 meV. Since when B is increased the third subband cannot propagate in the probes, we have only included the first two propagating subbands of the probes in our calculations throughout the whole magnetic-field range. Our calculated magnetocapacitances $C_{31}(\mathbf{B})$ (solid line) and $C_{32}(\mathbf{B})$ (dashed line) are shown in Fig. 2. These were obtained using Eq. (1) directly without using the dn_j, which includes the small potential correction dU. The data points in Fig. 2 were from the dn_j as described above. The two curves are consistent with each other. We have checked that the numerical difference between the data points and the approximate curves differ by $\sim 1\%$. We emphasize that this small change reflects the effect of dU on the injectivity: a small dU on top of the overall potential landscape $U(\mathbf{r})$ alters the injectivity slightly for the set of system parameters used here. On the other hand, the characteristic potential[1] $u_j(\mathbf{r}) \equiv e dU/d\mu_j$ plays a central role in setting up the induced charge and the polarization of the system. In our model such a charge polarization is treated classically for the large metal gate, as discussed above.

To reduce numerical effort, we have fixed the identical leads 1 and 2 at the middle of the square plate as shown in Fig. 1. Because of this geometric symmetry, transport from lead 1 to 2 at $-\mathbf{B}$ is equivalent to that from lead 2 to 1 at **B**. We thus have $C_{31}(-\mathbf{B}) = C_{32}(\mathbf{B})$. In the low-field regime $B = 0$–5000 G, $C_{31}(\mathbf{B})$, and $C_{31}(-\mathbf{B})$ $[C_{32}(\mathbf{B})]$ are quite different, displaying the remarkable asymmetry in the capacitances under magnetic-field reversal. This is clearly seen in Fig. 2. As mentioned above, such an asymmetry was observed in the experiments of Ref. 3. When values of B become larger, e.g., $B = 5000$–6900 G, while the asymmetry is still clearly observable, the general pattern of $C_{31}(\mathbf{B})$ and $C_{31}(-\mathbf{B})$ becomes similar. This is especially true for the positions and the shapes of the peaks as shown in Fig. 2.

Why does the capacitance behave this way? To understand we first notice that at large B there are regular and nearly equal-spaced peaks in both $C_{31}(\mathbf{B})$ and $C_{31}(-\mathbf{B})$. The spacing between these peaks is about $\Delta B \approx 400$ G, as seen in the inset of Fig. 2. From the area of the semiconductor plate, $S \approx 1.0 \times 10^{-9}$ cm^2, the magnetic flux passing through the plate is increased by $\delta\Phi = \Delta B S \approx 4 \times 10^{-7}$ G cm^2 when B is increased by ΔB. The fact that this value of $\delta\Phi$ is essentially a magnetic-flux quantum strongly indicates that the peaks in the capacitance C_{31} are due to Aharonov-Bohm (AB) type oscillations. To confirm this picture, in the inset of Fig. 2 we also plotted the reflection coefficient (dashed line) $r(\mathbf{B})$ for electrons coming in the first propagation mode. Clearly the capacitance undergoes a magnetic oscillation similar to that of the reflection coefficient. Their peaks are reached at the same field values. At high enough magnetic fields, the electron wave functions are ''pressed'' toward the walls of the quantum dot. In our case, at these high fields the semiconductor plate serves as a conducting ''ring'' that encloses a well-defined area. Consequently the transport coefficients undergo AB oscillations. The concurrence of the capacitance and the reflection coefficient peaks suggests this picture.

To further explore this possibility, we have examined a larger plate by doubling the area. For this larger system, in the magnetic-field range of 2640–3870 G which corresponds to a magnetic flux through the plate similar to that of the high-field range of Fig. 2, the capacitance has six large peaks with the following peak to peak distances: 240, 242, 284, 200, and 266 G. For a perfect metal ring, doubling the ring area reduces the AB oscillation period by a factor of 2. For our case, the oscillation period is reduced by a factor of ~ 1.6. This can easily be understood since our quantum dot is not a perfect ring, and the weaker field used for this larger system does not confine the electron wave to the edges of the quantum dot, thereby the effective area enclosed by a quantum path is less than doubled compared with that of the smaller quantum dot. Due to the weaker field the oscillation period is also less regular in comparison to those of Fig. 2. However the fact that the period is reduced by a factor of close to 2 when the quantum dot area is doubled gives another support that the nearly regular oscillation at the high field range of Fig. 2 is indeed due to Aharonov-Bohm effect.

To intuitively show this physical picture, in Fig. 3 we plot the norm of the wave function $|\Psi_1(\mathbf{r})|^2$ inside the scattering region, up to a constant this is the first subband contribution to the injectivity Eq. (2). At $B = 5494$ G which corresponds to a peak of C_{31} in the AB-oscillation region, Fig. 3(a) shows that $|\Psi_1(\mathbf{r})|^2$ has large values inside the semiconductor plate, with a pattern mimicking ''rings.'' On the other hand, for $B = 5126$ G which is not a peak position, Fig. 3(b) shows that $|\Psi_1(\mathbf{r})|^2$ is significant only along the direct path from probe 1 to probe 2. This confirms the physical picture discussed above. Finally, it is easy to understand why the peak shapes of $C_{31}(\mathbf{B})$ and $C_{31}(-\mathbf{B})$ become similar in the AB-

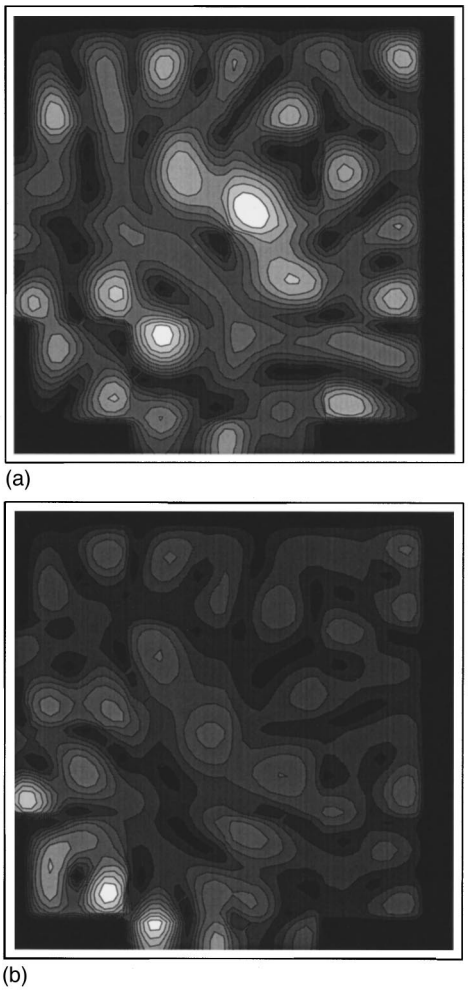

FIG. 3. The contour plot of the norm of scattering wave function at the first propagating subband inside the semiconductor plate. (a) For $B=5494$ G at which there is a peak in the quantum capacitance as shown in Fig. 2; (b) for $B=5126$ G at which the quantum capacitance takes a small value. Whiter regions indicate higher values of the norm.

oscillation region: the AB effect (the magnitude of the relative phases) is not sensitive to the direction of the magnetic field. The remaining difference in the magnitudes of $C_{31}(\mathbf{B})$ and $C_{31}(-\mathbf{B})$ is because of the difference in injectivities for the two different directions of **B**.

In summary, we have numerically applied the current-conserving and gauge-invariant AC-transport formalism to calculate the 3D mesoscopic capacitance of a three-probe system. Our numerical calculation shows that under a magnetic-field reversal, the capacitance for this three-probe capacitor is asymmetric. This is in qualitative agreement with the experimental result of Ref. 3, and confirms the general theoretical discussion of Ref. 4. In particular, the asymmetry is large at low fields. At high fields, an interesting result is that the capacitance undergoes Aharonov-Bohm type oscillations that effectively reduced the asymmetry of the shape of the oscillation peaks. Finally, for the small semiconductor quantum-dot system, the mesoscopic capacitance is small, in the fF range. In addition, under the assumption that the large metal gate responds classically, which allows us to approximate the induced charge on the metal gate using images, we have determined the potential change dU due to the scattering wave functions. Such a change alters the overall scattering potential landscape slightly and that modifies the charge injectivity. There are several further investigations to be made concerning the issues of quantum capacitance. The classical approximation used here for the metal gate drastically simplifies the numerical calculations. A natural next step is to solve Eq. (3) for the characteristic potential and the induced charge. This is a difficult problem since a Lindhard function, which describes the density response to a potential change, must be found for the scattering process. For metallic gates, this difficulty can be somewhat reduced using the Thomas-Fermi linear screening model. We expect the self-consistently determined characteristic potential to play an important role for situations where sharp junction resonances dominate the transport, and, more importantly, for cases where the two plates of the capacitor are both of mesoscopic sizes.

ACKNOWLEDGMENTS

The authors thank Professor M. Büttiker for several very useful communications that allowed us to clarify a number of conceptural issues concerning the quantum capacitance, and to fix an error in the unit of the injectivity. We would like to thank Xin Xue for a useful discussion. We gratefully acknowledge support by the Natural Sciences and Engineering Research Council of Canada, le Fonds pour la Formation de Chercheurs et l'Aide à la Recherche de la Province du Québec, a RGC grant from the Government of Hong Kong under Grant No. HKU 261/95P, and a research grant from the Croucher Foundation.

[1] M. Büttiker, Phys. Lett. A **180**, 364 (1993); J. Phys. (France) **5**, 9361 (1993); Phys. Rev. Lett. **57**, 1761 (1986).

[2] R. C. Ashoori *et al.*, Phys. Rev. Lett. **68**, 3088 (1992); T. P. SmithIII, W. I. Wang, and P. J. Stiles, Phys. Rev. B **34**, 2995 (1986); P. Lafarge *et al.*, Z. Phys. B **85**, 327 (1991).

[3] W. Chen *et al.*, Phys. Rev. Lett. **73**, 146 (1994).

[4] T. Christen and M. Büttiker, Phys. Rev. B **55**, R1946 (1997); **53**, 2064 (1996).

[5] Jian Wang and Hong Guo, Phys. Rev. B **54**, R11 090 (1996).

[6] M. Büttiker, A. Prêtre, and H. Thomas, Z. Phys. B **94**, 138 (1994).

[7] The induced charge in the equation of characteristic potential is the induced charge in the system caused by a change of the electrochemical potential at a contact.

[8] Yongjiang Wang, Jian Wang, Hong Guo, and E. Zaremba, Phys. Rev. B **52**, 2738 (1995).

[9] Although our calculation is only performed up to the Hartree level, it is not difficult to include other energies such as ex-

change and correlation by using standard density-functional theory. See, for example, Jian Wang, Yongjiang Wang, and Hong Guo, J. Appl. Phys. **75**, 2721 (1994); see also Ref. 8.

[10] C. S. Lent, J. Appl. Phys. **67**, 6353 (1990); Yongjiang Wang, Jian Wang, and Hong Guo, Phys. Rev. B **49**, 1928 (1994).

[11] M. Büttiker, Phys. Rev. B **38**, 12 724 (1988).

[12] Usually the scattering region is discretized using 3000 nodal points and we have carefully checked numerical convergence. See Ref. 10.